Journal of The Electrochemical Society, **160** (10) B201-B206 (2013)
0013-4651/2013/160(10)/B201/6/$31.00 © The Electrochemical Society

Chemical and Morphological Characteristics of ALD Al_2O_3 Thin-Film Surfaces after Immersion in pH Buffer Solutions

Joel Molina Reyes,[z] Berni M. Perez Ramos, Carlos Zuñiga Islas, Wilfrido Calleja Arriaga, Pedro Rosales Quintero, and Alfonso Torres Jacome

National Institute of Astrophysics, Optics and Electronics, INAOE, Tonantzintla, Puebla 72000, México

The chemical and morphological properties of thin aluminum oxide film surfaces (Al_2O_3 having 10 nm in thickness) in the as-deposited (dry) and after immersion (in pH buffer solutions) conditions were studied. Careful measurement conditions have been followed in order to determine any possible physical and/or chemical change on the surface of these films (after immersion in pH), so that proper correlation to their high and stable sensitivity to pH is possible. After deposition of thin Al_2O_3 films (by Atomic Layer Deposition, ALD) on chemically oxidized p-type silicon wafers, the resulting $Al_2O_3/SiO_X/Si$ stacked structures were characterized by Fourier-Transform Infrared Spectroscopy (FTIR) and Atomic Force Microscopy (AFM) before and after immersion in pH buffer solutions. Also, the Capacitance-Voltage (C-V) and Current-Voltage (I-V) characteristics were obtained after fabrication of Metal-Insulator-Semiconductor (MIS) devices in order to correlate the good chemical and morphological characteristics of thin Al_2O_3 to its electrical properties. Based on the characterization results, low surface oxidation/dissolution mechanisms are found in ALD aluminum oxide films when immersed in pH buffer solutions during short immersion times (immersion time $\leq$ 10 minutes); therefore, leading to the characteristic slow degradation of the sensitivity to pH for this dielectric material.
 [DOI: 10.1149/2.060310jes]

Manuscript submitted May 28, 2013; revised manuscript received July 19, 2013. Published August 16, 2013.

Ion-Sensitive Field-Effect Transistor (ISFET) devices, which are able to sense the activity of diverse chemical and biological species by transducing an electrochemical reaction into an electronic current, have a widespread use in these areas due to their micron-sized geometries (high integration density), fast speed of response and relatively low cost. Although they have many advantages, there are also various drawbacks to overcome. For instance, there is a considerable drift and hysteresis of ISFET response when it is operated in the long term under continuous conditions. These instabilities are usually related to the degradation of the chemical composition of the sensing layer (typically silicon nitride, Si_3N_4); i.e., oxidation degrades the commonly stable chemical response of the nitride layer to the unstable SiO_2;[1] also, hydration of the Si_3N_4 film could modify its dielectric properties in such a way that a more conductive surface layer is formed[2] and finally, saturation of the film's surface could occur from continuous adsorption of the chemical species of interest.[1]

On the other hand, for integration into useful electronic devices, these sensing materials must comply with a fully compatible Complementary Metal-Oxide-Semiconductor (CMOS) fabrication process, so that a low manufacturing cost of the final sensor can be obtained;[3–5] as a result, world research efforts are being focused into using novel dielectric materials as sensitive gates for ISFETs like stoichiometric Al_2O_3. Although aluminum oxide presents a high sensitivity to pH (close to the ideal Nernstian response),[2,6] neither the degradation mechanisms for an Al_2O_3-based ISFET (like sensitivity-drift) nor the initial ability of Al_2O_3 to give reliable pH measurements with high sensitivity are fully understood.[4,7] In this work, the chemical and morphological characteristics of ALD-Al_2O_3 have been examined in conditions where the surface of this oxide is exposed to pH buffer solutions for short periods of time. This way, this material is stressed using pH measurement conditions closely related to the real ones and whose results are then correlated to any significant changes in its physical properties before and after immersion in pH buffers of 4, 7 and 10. The obtained data indicates that stoichiometric Al_2O_3 films undergo low physical degradation after short-term (t $\leq$ 10 min of immersion) electrolyte-dielectric chemical interactions; thus correlating the great stability of Al_2O_3 for measurement of hydrogen activity to its original chemical bond densities and surface morphology.

Experimental

The bulk/surface chemical and physical characteristics of aluminum oxide films have been investigated using FTIR in absorbance mode with a Bruker Vector-22 system, AFM by NanoSurf EasyScan-2, as well as their electrical characteristics using high frequency C-V and direct current I-V measurements. For all samples, p-type ⟨100⟩ silicon wafers with a resistivity of ρ = 4–8 Ωcm were used. A 2.2–2.8 nm thick non-stoichiometric silicon oxide (SiO_X) was chemically grown on all the samples by introducing hydrophobic Si substrates (HF-last surfaces) in hydrogen peroxide (H_2O_2) solution heated at 80°C by 16 min. Then, aluminum oxide was deposited by ALD at 250°C using trimethylaluminum (TMA) and water as precursor gases with an average Al_2O_3 thickness of 10 nm. Also, MIS devices (for electrical characterization) were obtained by depositing 800 nm of aluminum film as gate electrode and 600 nm aluminum film as back electrode, both using E-beam evaporation. These MIS structures were used to determine the dielectric constant, total charge density, flatband voltage and hysteresis from high-frequency (100 KHz) C-V measurements, also electric field for breakdown Ebd, conduction mechanisms and hysteresis from I-V measurements.

On the other hand, three of the bare samples (having an $Al_2O_3/SiO_X/Si$ stacked structure without gate metallization) were measured by FTIR in order to determine their chemical composition (density of their chemical bonds) before and after immersion in pH buffers. They were first measured in the as-deposited condition (before immersion), then, they were subjected to sequential time-dependent immersion in pH buffer solutions, cleaning with deionized water (DI), drying, FTIR measurement, and immersion again. The whole cycle consisted of immersion in pH buffer (pH = 10, 7, and 4, from J.T. Baker) for 2 min, sample cleaning with DI and drying for 3 min; FTIR measurement and immersion again in pH buffer, see Figure 1a.

Another three bare samples were used for AFM imaging in contact mode, starting with the as-deposited measurement. Then, the samples were immersed in pH buffers for 10 min each, and measured again in order to record the sample's surface change when exposed to the pH solutions, see Figure 1b.

The electrical properties of bulk Al_2O_3 were obtained with a *Keithley Model 82-WIN* (for C-V measurements), using a voltage range from −5 to 5 V and a frequency of 100 KHz. I-V characteristics were obtained with an *HP-4155B Semiconductor Parameter Analyzer* (SPA), in a range from 0 to 40 V. All electrical measurements were done at room temperature.

Experimental Results

FTIR before immersion in pH buffer solutions.— Initially, the FTIR spectrum of the chamber's atmosphere and from a hydrophobic Si substrate were recorded and used as a subtraction reference in

[z]E-mail: jmolina@inaoep.mx

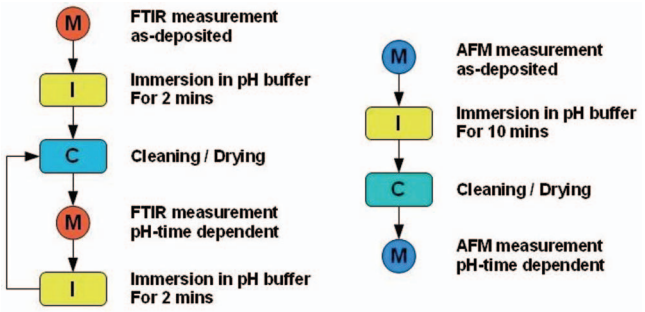

Figure 1. Experimental sequences for (a) FTIR (left) and (b) AFM (right) measurements in dependence with the immersion time.

order to reduce undesired features in the oxide spectra. After correction for the atmosphere contribution, the spectrums for all samples are found to be identical, with slight changes in the H_2O and CO_2 bands. Figure 2 shows the spectrum of $Al_2O_3/SiO_X/Si$ stacks before immersion in buffer solutions. An important number of absorbance peaks can be identified, the most relevant being: (1) 3716 cm^{-1}, (2) 1107 cm^{-1}, (3) 968 cm^{-1}, (4) 889 cm^{-1}, (5) 739 cm^{-1}, (6) 611 cm^{-1}, (7) 567 cm^{-1} and (8) 513 cm^{-1} which correspond, respectively, to the isolated surface AlO-H stretching vibrations,[8,9] ultra-thin chemically-grown SiO_2 transversal optic (TO) stretching mode,[10] Al-O longitudinal optic (LO) stretching,[9,10] condensed Al-O_4 tetrahedra,[11,12] Al-O TO stretching,[9,10] Al-O_2 TO bending,[11] and (7) and (8) correspond to stretching mode at condensed Al-O_6 octahedra.[11,12]

The aluminum oxide modes found are characteristic of amorphous vibrational modes, with exception of the 567 and 523 cm^{-1} centered bands which indicate that a fraction of the arrangement of the molecules in the Al_2O_3 layers might be microcrystalline. One discrete peak in the middle of the band, at 667 cm^{-1}, is due to the presence of CO_2.[10] The chemical designation for all peaks and their corresponding vibrational energies are presented in Table I.

FTIR after time-dependent immersion in pH buffer solutions.— In order to determine the relative change in the density of chemical bonds present in the dielectric films after immersion within pH buffer electrolytes, FTIR vs immersion time measurements were performed. Initially, the absorbance values around 968 cm^{-1} were fitted to a Gaussian and the obtained areas (after integration using the same range for wavenumber) are shown in Figure 3. We detected a slightly increased chemical reactivity of the oxide with acidic solutions in comparison with neutral and basic ones due that the magnitudes of the areas remain constant after immersion in solutions with pH 10 and 7, and they show a slight increase in the case of pH 4. This difference in the magnitude of the absorbance at 968 cm^{-1} is a qualitative result

Table I. Peak designation, wave number of the peak's maximum absorbance, and associated vibrational modes of the corresponding chemical bonds for the as-deposited FTIR spectrum of Al_2O_3/SiO_X /Si.

Number	Position [cm^{-1}]	Mode Type	Chemical Bond
1	3716	Stretching	AlO-H
2	1107	TO Stretching	Si-O
3	968	LO Stretching	Al-O
4	889	Condensed Tetrahedra	Al-O_4
5	739	Condensed Tetrahedra Stretching	Al-O_4
6	611	TO Bending	Al-O_2
7	567	Condensed Octahedra Stretching	Al-O_6
8	513	Condensed Octahedra Stretching	Al-O_6

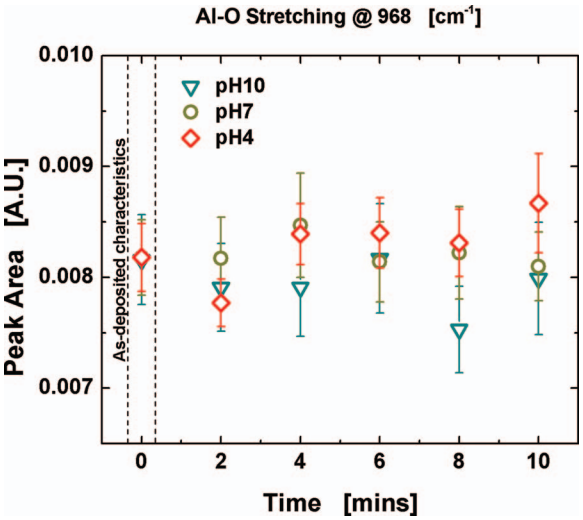

Figure 3. [Color online] Change in the adjusted absorbance peak (centered at 968 cm^{-1}) as a function of continuous immersion.

of the chemical interactions present in the top dielectric when it is in direct contact with the pH solutions.

It is important to highlight that the cleaning process (rinse in deionized water after pH buffer immersion and drying in pure nitrogen) does not affect the FTIR spectra in the bands of interest. Nonetheless, it has been observed that by this procedure the H_2O characteristic peaks increase monotonically with the immersion time (as expected),

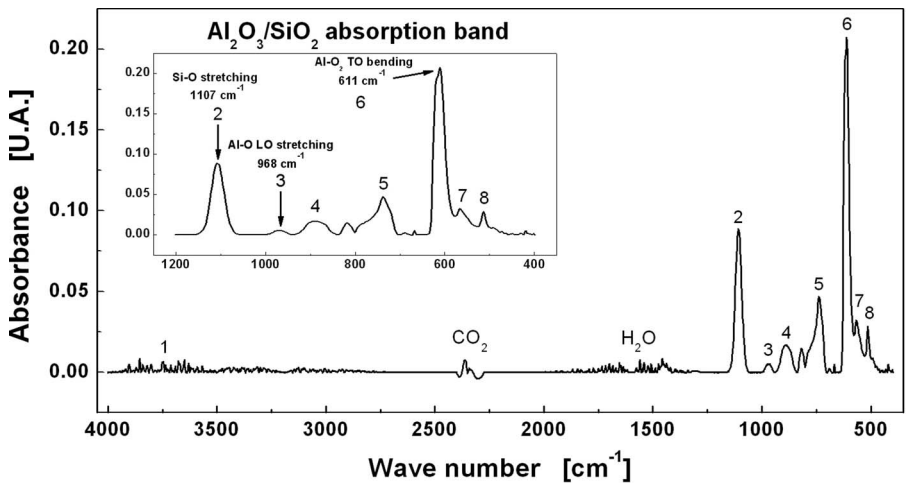

Figure 2. FTIR spectra of the as-deposited $Al_2O_3/SiO_X/Si$ stacks.

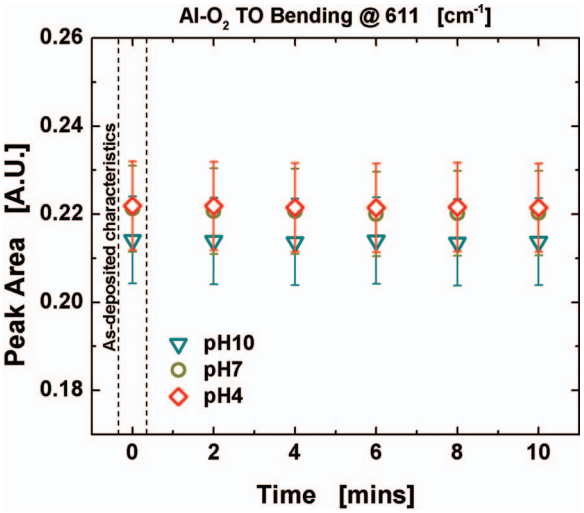

Figure 4. [Color online] Change in the adjusted absorbance peak (centered at 611 cm^{-1}) as a function of continuous immersion.

being these the only spectra differences that are directly related to the cleaning process.

Besides, the areas under the 611 cm^{-1} peak show a highly stabilized tendency after immersion in pH buffers as seen in Figure 4. Indeed, no change is detected in the absorbance area with respect to the initial measurements. Thus, the 611 cm^{-1} band has shown no sensitivity after 10 min of solution exposure and being the most relevant absorption peak for bulk aluminum oxide, we notice that the chemical integrity of the dielectric can be ensured for immersion in the short term.

Also, IR data for the Si-O chemical bond (mainly related to the interfacial oxide SiO_X) has been analyzed and it is shown in Figure 5. The area differences at the initial measurement (time equal to zero) between samples are caused by bond density variations on the chemically grown oxide due to its non-uniform nature.[13] Nevertheless, this specific bond presents constant absorbance characteristics after immersion in all pH buffers. This is expected since it would be hard that the solution could have reached the interfacial oxide and modified its chemical properties at such short immersion times.

Aside with the absorbance characteristics previously measured for bulk bands, changes in surface vibrational modes are of interest because they are directly related to the pH sensitivity of aluminum

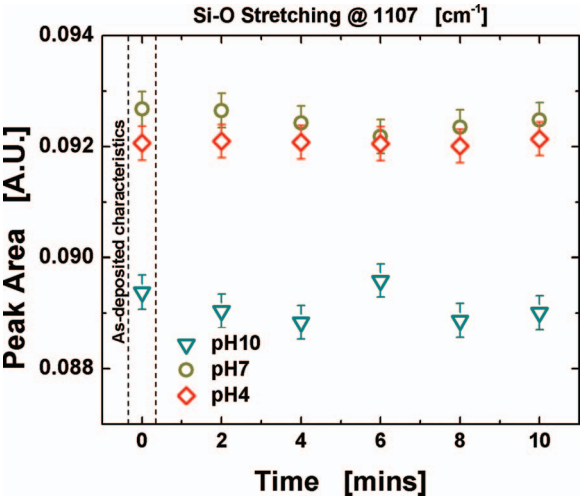

Figure 5. [Color online] Change in the adjusted absorbance peak (centered at 1107 cm^{-1}) as a function of continuous immersion.

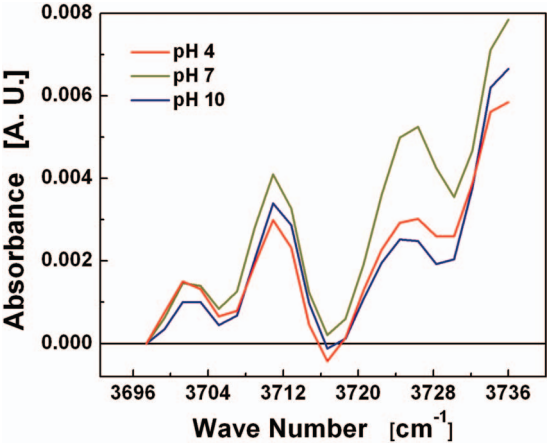

Figure 6. [Color online] Difference spectra of the AlO-H* band after 10 mins of immersion in buffer solutions.

oxide.[1,2,6,7] Changes in the chemical bond density related to surface sites have been monitored through the stretching vibrational modes of the isolated AlO-H* surface bond (the* denotes surface species) and which is located around 3716 cm^{-1}.[8,9] Figure 6 shows the difference spectra plots, obtained by subtracting the spectra of samples after immersion from the spectra of the bare samples, for the 3716 cm^{-1} centered band after sequential immersion in pH buffer solutions for 10 min. Difference spectra plots help to identify any possible gain or loss in the concentration of the species of interest after electrolyte immersion. It is thought that a negative absorbance characteristic (located around 3716 cm^{-1}) is related to a reduction in the density of surface AlO-H bonds ([AlO-H*]) after immersion in pH = 10 and 4 solutions. A relatively constant density concentration for the same chemical bond is found in samples exposed to pH = 7 solutions. These surface sites behave in a similar way to the bulk band located at 968 cm^{-1} after immersion (see Figure 3). In both cases, slightly higher chemical reactivity in their corresponding chemical bonds is found for pH = 4 when compared to neutral and basic solutions.

AFM in contact mode.— The surface morphology of the films has been investigated through AFM by measuring their surface roughness before and after immersion in pH buffers. All measurements were done by scanning an area of 500 × 500 nm in direct contact mode.

Figure 7 shows the AFM images for surface Al_2O_3 (surface of the $Al_2O_3/SiO_X/Si$ stack) before and after immersion in pH = 10 (left). We notice a very flat surface with small roughness, characteristic of ALD films.[14] The surface roughness (R_q) for this sample before immersion is 3.26 Å, and after immersion it is 3.84 Å.

Also shown in Figure 7 is the AFM image for surface Al_2O_3 before and after immersion in pH = 7 (center). Again, the surface roughness for this dielectric remains almost the same after immersion. The measured roughness for the as-deposited sample is R_q = 3.57 Å, while after immersion it is R_q = 3.37 Å.

The last sample, immersed in pH = 4 and also shown in Figure 7 (right), presents a surface roughness of Rq = 3.46 Å before, and Rq = 3.54 Å after immersion. It is interesting to notice that almost no change is detected for all samples (having the same Al_2O_3 on the surface) after immersion in pH solutions, whether acid or basic. Surface roughnesses for all samples are presented in Table II.

If present, morphological changes in surface roughness would have a direct impact in the capabilities of the oxide when used as sensing layer for chemical sensors like ISFET devices. Here, we show that the surface morphology of Al_2O_3 does not change to a big extent, so that the measured roughness after immersion is closely related to the characteristic roughness of the films in the as-deposited condition. In other words, these films do not have any appreciable reduction in

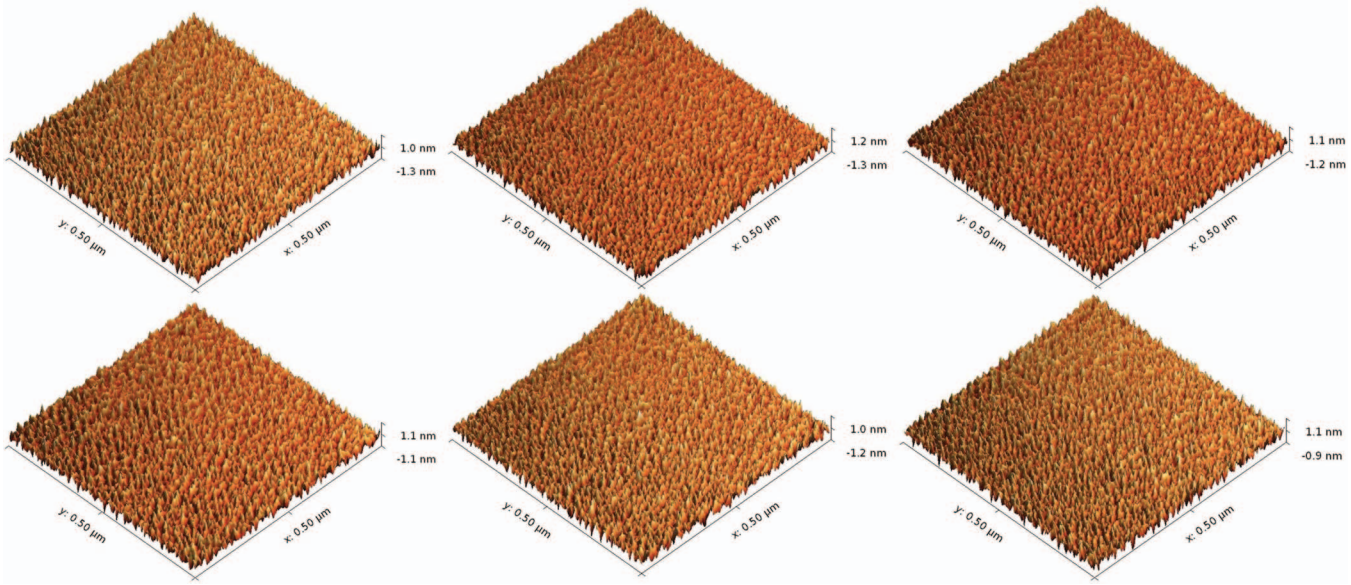

Figure 7. AFM images of Al_2O_3 film surface before and after immersion (top/bottom images respectively) in pH buffer solutions from left to right pH10, 7 and 4.

the short term and, because of the great stability to keep almost the same density of chemical bonds related to Al-O (see Figure 4), their chemical sensitivity to pH must remain almost constant when exposed to solutions during short immersion times.

Capacitance-voltage (C-V) characteristics.— In addition to the chemical and morphological characterization of thin Al_2O_3 as sensing material, we also have obtained its experimental C-V and I-V data in order to show that the high quality of Al_2O_3 is also present on its electrical characteristics. Specifically, thin Al_2O_3 is important for its good dielectric, interface and thermal stability properties (among many other parameters) so that Al_2O_3 is commonly used in advanced logic and memory applications having string electrical requirements.[15–18] Here, we just demonstrate how the electrical characterization applied to this material, relate well with an ALD Al_2O_3 having high-quality for pH sensing applications.

Single and dual-swept measurements were carried out so that the flatband voltage (V_{FB}), hysteresis, minimum/maximum capacitance, dielectric constant and total oxide charge density were estimated. The measured MIS devices have an $Al/Al_2O_3/SiO_X/Si/Al$ stacked structure and they were not annealed in forming gas. Figure 8 shows typical C-V characteristics of a MIS structure where the dielectric constant, maximum and minimum capacitance, and flatband voltage are: $\kappa_S = 5.65$ (at 100 KHz), $C_{OX} = 673$ pF, $C_{MIN} = 15$ pF, and $V_{FB} = -1$ V, respectively. We notice that the total dielectric constant is relatively low when compared to only Al_2O_3.[14,19] A low dielectric constant is obtained because this parameter is extracted from C-V data taken from a dual gate oxide Al_2O_3/SiO_X, so that the total dielectric constant should be at some value between 9 and 3.9 for Al_2O_3 and SiO_2 respectively.[19] On the other hand, the semiconductor surface is at moderate inversion at zero bias. It is well known that aluminum oxide layers exhibit net negative charge density when in direct contact to silicon substrates.[20,21] Here, net positive charges present at the SiO_X and its interfaces (with silicon substrate and Al_2O_3 film) contribute to a net displacement to the left in the flatband voltage. Since the SiO_X layer is in direct contact with the silicon substrate, the influence of some fixed charge density at the silicon oxide would largely displace or shift the V_{FB} to negative values. The combined net charge density per unit area near the Al_2O_3-SiO_X/Si interface is $Q_{eff} = 3.12 \times 10^{12}$ cm^{-2}.

Figure 9 shows the hysteresis window after C-V measurement. Hysteresis is caused by trapping and detrapping of carriers at defect sites in the insulator. The measured hysteresis at V_{FB} was below 100 mV. This moderate value is believed to have its origins during creation of defects mainly from SiO_X which is chemically grown on silicon.

Current-voltage (I-V) characteristics.— After fabrication of MIS devices, we have measured the electrical I-V characteristics of even thinner Al_2O_3 (with physical thickness of 6 nm after using simi-

Table II. Surface roughness before and after sample immersion in pH buffer solutions.

Sample	Roughness Before [Å]	Roughness After [Å]	% of Surface Change
pH10	3.26	3.84	+ 17.8
pH 7	3.57	3.37	−5.9
pH 4	3.46	3.54	+ 2.3

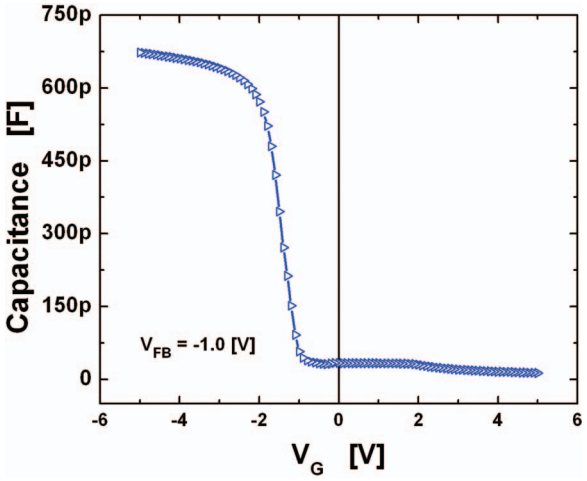

Figure 8. [Color online] High frequency C-V characteristics of a MIS capacitor using single-swept from inversion to accumulation.

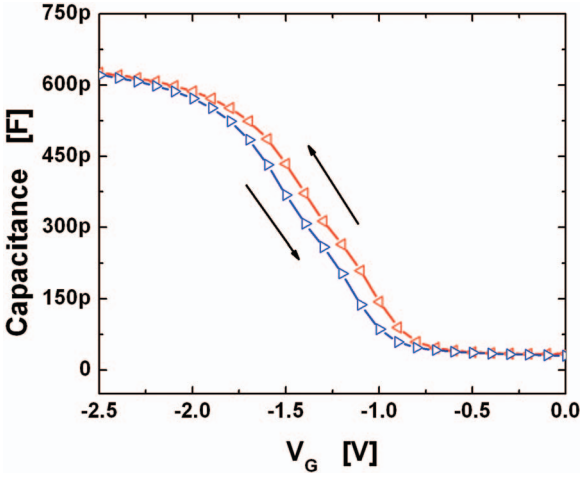

Figure 9. [Color online] High frequency C-V characteristics of a MIS capacitor using double-swept from inversion to accumulation and backwards.

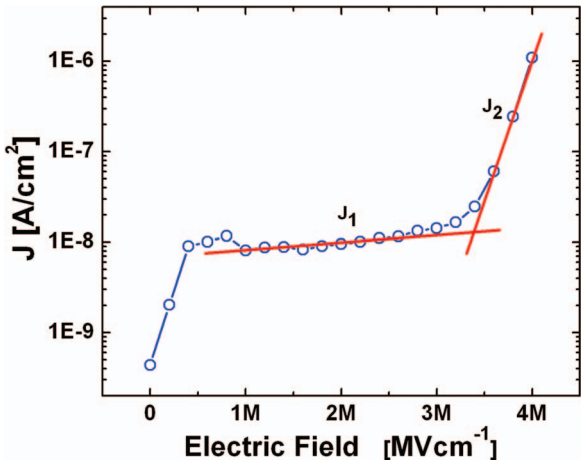

Figure 11. [Color online] J-E plot for a MIS capacitor (area of 13.44×10^{-4} cm^2) showing the dominant conduction regimes J1, J2.

lar ALD conditions and deposited directly on silicon) in order to corroborate good electrical uniformity of this material and thus, relate it to its outstanding chemical and morphological properties already presented. Figure 10 shows the gate current vs gate voltage after stressing several MIS capacitors ($Al/Al_2O_3/n$-Si system) until the gate dielectric reaches breakdown. We can see a high uniformity in the I-V characteristics (including breakdown voltage) because of the high quality of the ALD technique that produces excellent oxide thickness uniformity at the atomic level.[14] Initially, we notice that all MIS capacitors present a constant and low gate current level until it increases after $V_G \sim 2$ V (mainly by quantum mechanical direct-tunneling mechanism).[22] Later, hard breakdown is reached for all devices at almost the same applied gate voltage of $V_G \sim 4.45$ V, thus demonstrating not only a high uniformity on their electrical conduction mechanisms but also, on their dielectric breakdown characteristics as well.

On the other hand, additional I-V measurements were performed in order to determine hard hysteresis, breakdown field (E_{bd}) and the main conduction mechanism in the MIS system. Extracted $E_{bd} = 4.4$ MVcm^{-1}, which is in accordance with similar values reported in literature.[14] Higher E_{bd} values could be found in oxides having low density of intrinsic and extrinsic defects like pinholes or any other undesirable defect. The main conduction mechanisms are labeled in Figure 11 as J1 and J2. At low electric field, the conduction is direct-tunneling limited J1.[20,21,23] At higher fields (yet still below the breakdown field) Frenkel-Poole emission is dominant, J2.[20,21,23] Conduction behavior in Al_2O_3 is mainly determined by traps inside the insulator which, in our case, are generally filled with electrons (by a substrate injection mechanism) as observed by the reduction in gate leakage current density in Figure 12.

Additionally, the conduction mechanisms are highly sensitive to the deposition technique, thermal treatments after deposition of the gate oxides, film composition and thickness[20] so is quite important to ensure a reproducible deposition technique for the gate oxide in order to minimize every possible source of electrical variation (or sensitivity to pH when Al_2O_3 is used for ion detection). In particular, the high thermal stability of ALD Al_2O_3 has been already demonstrated and applied to the development of advanced gate oxide stacks in logic and memory applications[24,25] based on these high dielectric constant (high-k) materials.

Since the Al_2O_3 thickness is thick enough (10 nm) to reduce direct tunneling, its conduction regime is thought to be trap-assisted tunneling, TAT. In the high field regime, the gate current might originate because of field enhanced thermal excitation of oxide-trapped electrons into the conduction band.[20,23] In both conduction regimes, the I-V characteristics denote the presence of traps in a wide range of electric field. Finally, the hysteresis behavior shown in Figure 12 is caused by a net injection of both carriers (electrons and holes) creating a redistribution of internal fields which ultimately leads to a reduction

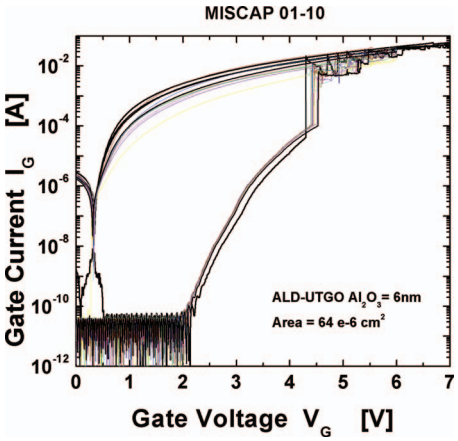

Figure 10. [Color online] I-V characteristics of MIS capacitors with ~ 6 nm thick ALD aluminum oxide film.

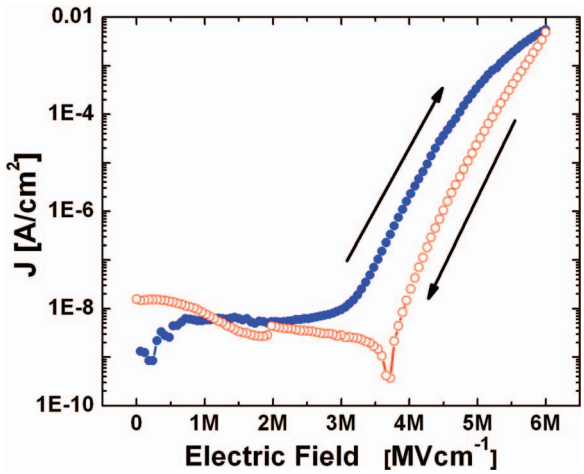

Figure 12. [Color online] Hysteresis behavior for a fresh MIS capacitor during substrate injection.

in leakage current. The magnitude of the I-V hysteresis in these films highlights the presence of low interface defects' density.[20]

Discussion

Aluminum oxide is an amphoteric material,[26] which means that reactions of surface Al-OH* sites with H^+ or OH^- ions from contact with electrolytic solutions lead to the formation of positive Al-OH_2^+, or negative Al-O^- charges on the surface and that depends on the pH of the solution. These reactions are explained by the site-dissociation/site-binding theory.[2,7,27,28] The chemical parameters of interest for application of ALD Al_2O_3 as sensing layer in pH sensors are the total density of surface sites at the electrolyte/oxide interface (N_S) and the surface chemical reactivity determined by the apparent association constants of protons with Al-OH*. By means of FTIR and AFM measurements, chemical and morphological characteristics on the top oxide layer were obtained and compared.[10,29] These results suggest that it should not be an appreciable decrease in chemical sensitivity of the Al_2O_3 layer after short immersion times using electrolytes with pH = 7 to 10. The strongest chemical interactions occur when the films are immersed in highly acidic solutions (pH = 4), as can be inferred from the changes in surface bonds density recorded with FTIR. AFM results support the chemical stability of aluminum oxide by recording negligible changes in surface roughness. Also, the ALD oxide films are low in defect/pinholes densities,[9,11,14] which prevent solubility of Al_2O_3 with the electrolyte and slow the diffusion of electrolyte subproducts.[2,30,31] The bottom line is that the surface reduction of Al_2O_3 is negligible in the whole range of pH tested (from 10 down to 4).[26] Near pH = 4 the dissolution becomes slightly perceptible but the surface's chemical reactivity of Al_2O_3 remains constant in short immersion times, therefore suggesting that this specific material has well enough physical and chemical properties for use in reliable pH detection applications and with nearly ideal Nernstian response.[2,6,27]

Conclusions

The chemical stability and surface roughness characteristics of thin Al_2O_3 films were found to be slightly affected after direct contact to pH electrolytes at short immersion times. After MIS device fabrication, these films (in series with an ultra thin SiO_X layer) also showed good electrical characteristics after C-V and I-V measurements. In brief, ALD Al_2O_3 films are well suited for pH sensing applications in the pH range of 10-4 and short-time measurements given their good stability in terms of their chemical and morphological characteristics.

References

1. T. Mikolajick, R. Kühnhold, R. Schupp, and H. Ryssel, *Sensors and Actuators B: Chemical*, **58**, 450 (1999).
2. M. Madou and S. Morrison, *Chemical Sensing with Solid State Devices*, Academic Press, San Diego (1989).
3. L. Bousse, J. Shott, and J. D. Meindl, *IEEE Electron Device Letters*, **9**, 44 (1988).
4. T. Prodromakis, Y. Liu, T. Constandinou, P. Georgiou, and C. Toumazou, *IEEE Electron Device Letters*, **31**, 1053 (2010).
5. J. Molina, A. Torres, G. Espinoza, M. T. Sanz, E. Guerrero, B. Perez, J. Fernandez, M. Hoque, and P. Parris, *Procedia Chemistry*, **6**, 110 (2012).
6. J. Janata and R. Huber, *Solid State Chemical Sensors*, Academic Press, Orlando (1985).
7. Y. G. Vlasov, Y. a. Tarantov, and P. V Bobrov, *Analytical and bioanalytical chemistry*, **376**, 788 (2003).
8. J. Ferguson, A. Weimer, and S. George, *Chemistry of materials*, **16**, 5602 (2004).
9. D. N. Goldstein, J. A. McCormick, and S. M. George, *The Journal of Physical Chemistry C*, **112**, 19530 (2008).
10. V. Tolstoy;, I. Chernyshova;, and V. Skryshevsky, *Handbook of Infrared Spectroscopy of Ultrathin Films*, John Wiley & Sons, New York (2003).
11. R. Katamreddy, R. Inman, G. Jursich, A. Soulet, and C. Takoudis, *Journal of The Electrochemical Society*, **153**, C701 (2006).
12. P. Tarte, *Spectrochimica Acta Part A: Molecular Spectroscopy*, **23**, 2127 (1967).
13. S. Petitdidier, V. Bertagna, N. Rochat, D. Rouchon, P. Besson, R. Erre, and M. Chemla, *Thin Solid Films*, **476**, 51 (2005).
14. S. M. George, *Chemical reviews*, **110**, 111 (2010).
15. M. Groner, J. Elam, F. Fabreguette, and S. George, *Thin Solid Films*, **413**, 186 (2002).
16. G. D. Wilk, R. M. Wallace, and J. M. Anthony, *Journal of Applied Physics*, **89**, 5243 (2001).
17. L. Miotti, R. P. Pezzi, M. Copel, C. Krug, and I. J. R. Baumvol, *Applied Physics Letters*, **90**, 052913 (2007).
18. J. B. Kim, D. R. Kwon, K. Chakrabarti, C. Lee, K. Y. Oh, and J. H. Lee, *Journal of Applied Physics*, **92**, 6739 (2002).
19. V. Mikhaelashvili, Y. Betzer, I. Prudnikov, M. Orenstein, D. Ritter, and G. Eisenstein, *Journal of Applied Physics*, **84**, 6747 (1998).
20. S. Dueñas, H. Castán, H. García, and L. Bailón, in *Dielectric Material*, M. A. Silaghi, Editor, p. 213–250, InTech, Rijeka (2012.).
21. C. M. Tanner, Y.-C. Perng, C. Frewin, S. E. Saddow, and J. P. Chang, *Applied Physics Letters*, **91**, 203510–1 (2007).
22. B. Han, S. W. Lee, K. Park, C. O. Park, S. K. Rha, and W. J. Lee, *Current Applied Physics*, **12**, 434 (2012).
23. M. Sze, *Physics of Semiconductor Devices*, John Wiley & Sons, New York (2006).
24. H. S. Chang, S. Jeon, H. Hwang, and D. W. Moon, *Applied Physics Letters*, **80**, 3385 (2002).
25. B. Veith, F. Werner, D. Zielke, R. Brendel, and J. Schmidt, *Energy Procedia*, **8**, 307 (2011).
26. E. Tombácz, Á. Dobos, M. Szekeres, H. Narres, E. Klumpp, and I. Dékány, *Colloid & Polymer Science*, **278**, 337 (2000).
27. L. Bousse, N. F. De Rooij, and P. Bergveld, *IEEE Transactions on Electron Devices*, **30**, 1263 (1983).
28. D. Yates, S. Levine, and T. Healy, *Journal of The Electrochemical Society, Faraday Transactions 1*, **70**, 1807 (1974).
29. P. Christensen and A. Hamnett, *Electrochimica Acta*, **45**, 2443 (2000).
30. S. Jamasb, S. D. Collins, and R. L. Smith, *IEEE Transactions on Electron Devices*, **45**, 1239 (1998).
31. S. Jamasb, S. D. Collins, and R. L. Smith, *9th Int. Conf. Solid-State Sensors and Actuators (Transducers '97)*, **2**, 1379 (1997).